EXAMINATION OF THE POSSIBILITY TO SUPPRESS BACKGROUND FLUORESCENCE SIGNALS FROM WATER RELEVANT TO THE PROBLEMS OF OIL FILMS REMOTE DETECTION

V.M. Klimkin and V.N. Fedorishchev

Institute of Atmospheric Optics,
Siberian Branch of the Russian Academy of Sciences, Tomsk
Received May 17, 1994

The possibility of suppressing signals from water subjacent layer is analyzed numerically in connection with the problem on remote detection of oil films by laser-induced fluorescence spectra. The gain in temporal resolution of the instrument up to 1 ns is shown to produce only insignificant gain in the signal-to-noise ratio. Essentially better results may be obtained by using a bistatic scheme of sounding. A simple way to calculate the optical arrangement of the fluorometer is described in the paper.

INTRODUCTION

Background water fluorescence of organic and mineral admixtures of different origin is one of the factors that limit sensitivity of a remote spectrofluorometer used for detection and analysis of thin films of oil spills on water surface.[1] Although the content of admixtures in natural water is, as a rule, not very high, the presence of background signals is connected with the significant thickness of water layer irradiated by a laser pulse (1-10 m) as compared to the typical thickness of the films to be detected (1-10 μm). Variations in the film position resulting from water roughness is an important specific feature of the film as an object for remote sensing.

To suppress the background signal, it is necessary to decrease the thickness of water layer in order to reduce fluorescence light coming to a fluorometer. This can be done by either improving a detector temporal resolution or spatial selection as, for instance, in the case of a bistatic scheme of a transceiver.

In this paper, a numerical analysis of signals detected with a fluorescent lidar is made to evaluate the efficiencies of both methods to suppress the background.

1. COMPUTATION AND ANALYSIS OF SIGNALS DETECTED WITH A REMOTE SPECTROFLUOROMETER IN A MONOSTATIC OPTICAL ARRANGEMENT OF SOUNDING

Assume that the signal detected is a sum of a signal from a thin oil film $F(t)$ and the background water fluorescence signal $B(t)$. Let the background fluorescence be determined by luminescence of phytoplankton and dissolved organic matter (DOM) distributed homogeneously over the water depth. Let us denote the total absorption coefficient as k, the water absorption coefficient as C, and the absorption coefficients at the laser wavelength as k_L and C_L, respectively. The oil fluorescence will be described by quantum efficiency φ_f and decay time τ_f. The corresponding parameters of the background fluorescence will be φ_b and τ_b.
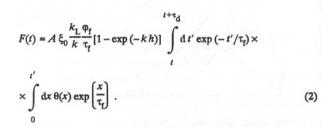
Then the expression for the energy of the background fluorescence signal received by a spectrofluorometer during the time interval $(t, t + \tau_d)$ can be written as[2]

$$B(t) = A \exp(-kh) \frac{\varphi_b C_L}{\tau_b} \int_t^{t+\tau_d} dt' \int_0^H dH' \xi(H') \times$$
$$\times \exp\left(CH' - \frac{t'}{\tau_b}\right) \int_0^{t'} dx\, \theta(x) \exp\left(\frac{x}{\tau_b}\right). \qquad (1)$$

Here A is a constant, e. p$(-kh)$ describes the extinction of radiation by the oil film, $\theta(x)$ is the laser pulse shape, H is the sounding depth connected with the length of time interval by the following equation: $H = ct/2n$ (c is the speed of light, n is water refractive index), τ_d is the time constant of detection, and $\xi(H)$ is geometrical function of the receiving system.

When deriving Eq. (1), the following fact was taken into account. At time moment t, when the leading edge of laser pulse reaches the depth tf, the radiation from the upper depths also falls onto the detector due to a finite duration of the laser pulse and "lengthening" of fluorescence decay process in time.

For the signal from oil film, whose thickness h is negligible as compared to the depth of a laser pulse penetration, the integrals over depth and over time can be separated and expression (1) can be reduced to

$$F(t) = A \xi_0 \frac{k_L}{k} \frac{\varphi_f}{\tau_f} [1 - \exp(-kh)] \int_t^{t+\tau_d} dt' \exp(-t'/\tau_f) \times$$
$$\times \int_0^{t'} dx\, \theta(x) \exp\left(\frac{x}{\tau_f}\right). \qquad (2)$$

Here ξ_0 is the geometrical function at the film surface.

In calculations wc assume that the laser pulse shape is described by the following function[2]:

$$\theta(t) = (t/\tau_0)^n \exp(-t/\tau_0) / [\tau_0 \, \Gamma(n+1)] \qquad (3)$$

at $n = 2$. In Eq (3) τ_0 is the characteristic time of the laser pulse (the maximum amplitude is reached at $t = n\tau_0$), Γ is the gamma-function.

For certainty, we use parameters inherent in a spectrofluorometer described in Ref. 1. Let $\tau_0 = \tau_d = 1$ ns. The values k_L and κ for crude oil are also taken from Ref. 1, whereas C_L and C values are calculated for a phytoplankton concentration of 10 mg/m^3 based on data from Ref. 3. They correspond to the laser wavelength of 355 nm. In order to simplify the interpretation of data let us take A, φ_f, and φ_b factors as well as the ξ value to be equal to unity. The decay time of phytoplankton fluorescence is taken to be $\tau_b = 1$ ns, and the decay time of oil fluorescence is considered to be $\tau_f = 1$ and 10 ns. The time profile of the signal was computed with a step $\Delta t = 1$ ns that corresponds to spatial resolution in water of 0.1 m. It should be noted that real fluorescence signals are longer since they are a convolution of the expressions like Eq. (1) or (2) with the instrumental function of a receiving system.

Figure 1 presents the profiles of fluorescence signals calculated for an oil film 0.5 μm thick on water surface. Both the net signal $S(t)$ and its components $F(t)$ and $B(t)$ are shown there. In this case, $\tau_f = \tau_b = 1$ ns. Net signals for different film thicknesses are presented in Fig. 2. The family of curves I in Fig. 2 relates to the case of $\tau_f = 1$ ns, and the family II is plotted for $\tau_f = 10$ ns. In the first case, the shape of a curve depends strongly on the film thickness and, therefore, can be used for separation of signals from the film in the presence of background fluorescence. By employing a fast analog-to-digital converter for its recording one can, for instance, determine the ratio between the signals at different time moments or calculate the correlation of the signal with a certain standard signal. As is seen from Fig. 2, the situation is much more complicated for oil products with long fluorescence decay time. However, it should be mentioned that in this case the ratio of amplitudes of signals detected at subsequent moments changes with the film thickness too
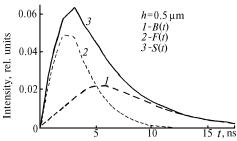
FIG. 1. Calculated signals from the water (1), a film (2), end total signal (3).
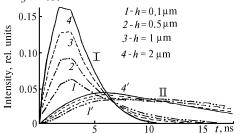
FIG. 2. Calculated signals recorded with the fluorometer for oil products with short ($\tau = 1$ ns) (I) and a relatively long decay time ($\tau = 10$ ns) (II) for the films of different thickness.

2. GEOMETRICAL FUNCTION OF A BISTATIC OPTICAL SYSTEM

When writing a lidar equation it is usually assumed that the signal value decreases proportionally to the square of the distance to a target. However, as is shown in Ref. 2, the use of small–size detectors or field of view diaphragms (for instance, fiber waveguides) leads to the losses in optical signal from the near portions of the path and, as a result, the signal is a complicated function of distance for short and medium paths. This effect can be taken into account by introducing the lidar geometrical function (GF). The fluorometer GF calculation for oil film detection can be useful also for minimization of the background fluorescence from water. The optical system of such a fluorometer should record the signal from as small water volume as possible. As we have already mentioned, the bistatic sounding scheme with spatial separation of the optical axes of transmitting and receiving objectives, provides more or less satisfactory solution to this problem.

Let us consider an optical system that consists of a transmitting objective L_1 and a receiving objective L_2 conjugated with the fiber optical waveguides (see Fig. 3). Let the image of the transmitting fiber end be focused on a target surface at a distance R_1 from the transmitting lens plane, whereas the image of the receiving fiber be focused to the point located at a distance R_2 along the x axis (see Fig. 3). Let us denote radii of the output apertures of the objectives by r_0 and ρ_0 and their focal lengths by f_{12}, d_0 is the distance between the axes of the objectives, the beam cross section at a distance x from the focal plane is designated by r_x, and the fiber ends radii by r_d and ρ_d.
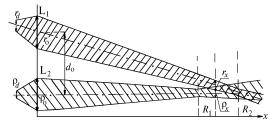
FIG. 3. On the calculation of the geometric function.

Because of mode mixing we can consider that the homogeneously illuminated end of a monofiber waveguide is a source of laser radiation and laser radiation leaving objective obeys the laws of geometrical optics. Let us introduce dimensionless parameters $z_1 = x/R_1$, $W_1 = R_1/f_1$, and $N_1 = \rho/\rho_d$. Then the laser beam profile along its axis can be written as

$$\frac{\rho(z_1)}{\rho_0} = \frac{W_1 - 1}{N_1} z_1 + \theta(z_1)(z_1 - 1), \qquad (4)$$

where

$$\theta(z) = \begin{cases} 1 & \text{for } z \geq 1, \\ -1 & \text{for } z < 1. \end{cases}$$

Similar expression can be written for the receiving telescope field of view. The recorded signal is proportional to the coefficient ξ characterizing spatial overlapping of the transmitted and received beams.[2] The image of a profile cross section for field of view of receiving objective at an arbitrary point z_2 forms a scattering circle of r_d' radius in the plane of end of receiving fiber waveguide

$$r_d' = r_d + 2\,\theta(z_2)\,(r_0/z_2)\,(z_2-1)\,/\,(W_2-1)\,. \qquad (5)$$

It is evident that $r_d \le r_d'$ and, hence, only a part of the signal energy from the region of beam overlapping reaches the detector through the fiber. Let us introduce the image transfer ratio ξ_2 as

$$\xi_2(z_2) = r_d^2 \,/\, r_d'^{\,2}\,. \qquad (6)$$

Then the net geometrical function of transceiving system is determined by a product of coefficients of beam overlapping and image transfer ratio and we have (assuming $z_1 = z_2 = z$)

$$\xi(z) = \xi_1(z)\,\xi_2(z)\,. \qquad (7)$$

To analyze the expression (7), we have carried out calculations of the GF for some typical configurations of transceiving system. Telescope configuration presented in Ref. 1 was taken as the basic one (all dimensions, except as otherwise noted, are represented in millimeters): $\rho_0 = 45$, $r_0 = 33$, $f_1 = 450$, $f_2 = 300$, $\rho_0 = 0.4$, $r_d = 0.125$, and $d_0 = 85$. In these calculations we assumed that the target plane was located at $z_1 = 1$, the receiving objective was focused at $z_2 = z_1 + \Delta z$, where z_1 and z_2 are related as follows: $z_2 = z_1 \, R_1/R_2$

Figure 4 illustrates GF formation for the above lidar configuration at $\Delta z = 0.1$ and $R_1 = 25$ m. Figure 5 presents geometrical function for the same configuration at $\Delta z = 0$ for different sounding depths. One can see that sounding depth affects only the width of GF. According to our estimations, the width of the GF is approximately proportional to sounding depth and receiving fiber radius and inversely proportional to the receiving objective diameter and its focal length.

Defocusing of transmitting and receiving objectives leads to transformation of GF from a single– to a double-peaked curve and to the shift of this curve with respect to $z = 1$. The amplitude and the width of the curve are larger for $\Delta z > 0$ than for the same value of a negative shift. For small sounding depths, defocusing results in a dramatic drop of GF value, whereas at $R = 25$ m only broadening of the curve maximum occurs, that is equivalent to increase of the depth of field of the telescope.
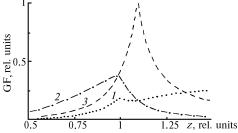

FIG. 4. Formation of the geometrical function for a bislatic two-lens transceiving objective: the resultant GF (1), beam overlapping coefficient (2), and image transfer ratio (3).
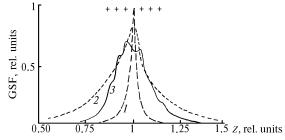

FIG. 5. Examples of geometrical Junctions: for sounding depth of 5 m and for a single–lens receiving objective (1), for sounding depth of 25 m and a single-lens receiving objective (2), for a 6–lens objective and sounding depth of 5 m (3).

As our calculations show, at $\Delta z = 0$ the maximum GF value is reached at $f_1/f_2 > 1$ since in this case the whole laser spot falls within the field of view of the receiving objective. The relative width of geometrical function $\delta z/\xi_{max}$ reaches its minimum at $f_1 = f_2$, hence, in this case defocusing of the objectives influences GF value most strongly. Therefore, when choosing the focal lengths of the objectives one should meet the condition $f_1 \ge f_2$ in order to obtain the maximum GF value. Moreover, the closer are f_1 and f_2, the narrower is the relative width of GF and the smaller is the depth of field of the telescope. The same regularities in GF behavior are observed when fibers radii are varied. In this case it is necessary to meet the condition $r_d > \rho_d$.

Figure 5 shows that for small sounding depths the GF is close to δ–function and even small displacement of the target plane relative to the objectives focal plane leads to a dramatic drop of the GF value and, therefore, the signal. Indeed, at $R = 5$ m if $d\,r$ is equal to 0.05, e.g., ± 25 cm, the signal decreases by a factor of five. At $R = 25$ m the same reduction of the signal is observed at a displacement of the planes by ± 5 m. Hence, to make the receiving system less sensitive to the displacement of a target and focus planes, the transmitting and receiving objectives should be defocused. The resulting from this decrease of the maximum value of GF will obviously be compensated for by an increase in the receiving objective area. However, in this case the $\xi(z)$ function becomes narrower. Therefore, it is reasonable to replace one large receiving objective by a set of objectives of smaller diameter with the same total area. Besides, separate focusing of each objective allows the optimal GF profile to be formed.

Curve 3 in Fig. 5 being the geometrical function for the system of six receiving objectives arranged axisymmetrically across the central transmitting objective illustrates the above said. Focal points of each objective are marked by crosses in the upper part of the figure. Fitting the focal-point locations for each objective, it is possible to obtain the GF profile with a sufficiently smooth top.

3. CALCULATION AND ANALYSIS OF REMOTE SPECTROFLUOROMETER SIGNALS FOR A BISTATIC SOUNDING SCHEME

As was shown above, the analysis of temporal profile of recorded fluorescence signal provides only limited possibility of extracting the informative part of the signal from oil-product films. At the same time, the shapes of fluorescence signals from the water and from the oil-product films differ noticeably. Therefore, it is interesting to analyze the possibility of separating these signals. Consider now an optical system that consists of one transmitting and two receiving objectives (see a fragment in Fig. 6). Let the transmitting and one of the receiving objectives be focused at the film surface, whereas another receiving objective be focused below the water surface. In this case, as follows from the analysis of geometrical function, the signal-to-background ratio reaches its maximum in the first channel and the second channel records mainly background water radiation that can serve as a reference for the first channel.

Figure 6 presents the temporal profiles of the signals in the informative (curve family I) and background (curve family II) channels that arc calculated from Eqs. (1) and (2) taking into account the geometrical function. Signals correspond to different thickness of oil-product films with short fluorescence decay time ($\tau \sim 1$ ns). It is assumed that planes of receiving objectives focusing are displaced by 0.5 m and the sounding depth is 5.25 m. Parameters of the optical system described in the previous section were used in

these calculations. As follows from Fig. 6, for oil products with short t the amplitude ratio of the signals in the two channels changes from 1 without film to 2.5 with film of h = 25 μm thikeness. For oil products with long τ the signal—to—noise ratio is lower but it can be increased by defocusing the objectives or by using larger spacing between them.
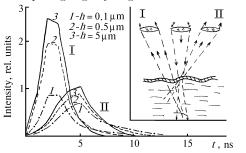

FIG. 6. Calculated signals for a bistatic sounding scheme: signals in the informative channel (I) and signals in the channel recording the background fluorescence (II).

CONCLUSION

Thus, suppression of background signal from water in the problem of remote sensing of oil—product films based on their fluorescence is a rather complicated problem. The analysis of two possible methods of signal—to—noise ratio improvement demonstrated the following.

A method oriented to high temporal resolution of the instrumentation has great potentials for detection and analysis of oil-product films with short fluorescence decay time τ. This method is inefficient for oil products with long τ. It should be taken into account that high temporal resolution of the order of 1 ns and higher requires a more complicated instrumentation of a fluoromeler.

A method of spatiotemporal analysis oriented to the bistatic sounding scheme enables one to achieve high signal-to-background ratio even with instrumentation exhibiting substantially low temporal resolution. At installation of the fluorometer onboard a ship the performance of this method is not difficult. However, the problems can appear if the fluorometer is installed onboard an aircraft. In particular, even for the flight at lower boundary of the altitude region, suitable for such experiments (50 m for a helicopter), it is necessary to develop a vibration—resistant holders for objectives with the spacing between them of 1 m and more.

REFERENCES

1. V.M. Klimkin, V.G. Sokovikov, and V.N. Fedorishchev, Atmos. Oceanic Opt. **6**, No. 2, 115-123 (1993).
2. R. Mezheris, *Laser Remote Sensing* (John Wiley and Sons, New York, 1987).
3. V.M. Orlov, LV. Samokhvalov, M.P. Belov, et al., in: *Remote Control of the Upper Oceanic Layer* (Nauka, Novosibirsk, 1991), pp. 124-136.